Dependence of electron dynamics on magnetic fields in semiconductor superlattices*

Yang Gui(杨 癸)[a)†], Wang Lei(王 磊)[b)], and Tian Jun-Long(田俊龙)[a)]

[a)] College of Physics & Electrical Engineering, Anyang Normal University, Anyang 455000, China
[b)] School of Mathematics and Physics, Anyang Institute of Technology, Anyang 455000, China

(Received 26 January 2013; revised manuscript received 18 April 2013)

Numerical simulation results are presented for a drift-diffusion rate equation model which describes electronic transport due to sequential tunneling between adjacent quantum wells in weakly coupled semiconductor superlattices (SLs). The electron dynamics is dependent on the external magnetic field perpendicular to the electron motion direction, and a detailed explanation is given. Using different parameters, the system shows different dynamic behaviors, and three distinct phenomena are observed and controlled by increasing magnetic field. (i) For a lower doping density, the system state transfers from stable state to oscillationary state. (ii) An opposite result is obtained to that in the case (i) for an intermediate value of the doping density, and the state changes from oscillationary to stationary. (iii) The state varies between oscillationary and stationary when doping density is large. Then, a detailed theoretical analysis is given to explain these surprise phenomena. The distribution of the electric-field domain along the SLs is plotted. We find the structure of the domain is almost uniform for a lower doping density, and no domain occurs in the SLs. By adding an external ac signal, complex nonlinear behaviors are observed from the Poincaré map and the corresponding phase diagrams when the driving frequency changes.

Keywords: superlattices, current oscillation, electric-field domain

PACS: 73.50.Fq, 72.20.Ht, 05.45.–a **DOI:** 10.1088/1674-1056/22/12/127305

1. Introduction

Even 40 years after the pioneering work by Esaki and Tsu,[1] semiconductor superlattices (SLs) are still a hot topic of research. SLs, comprising alternating layers of different semiconductor materials, provide a flexible environment for studying quantum transport.[2–10] Electrons in semiconductor SLs exhibit a wide range of nonlinear effects under external fields.[11–14] These are of fundamental scientific interest and useful for applications in ultrafast electronics. Presently the following directions stand out: SLs with lower dimensions,[15] generation of THz signals,[16] self-sustained current oscillations (SSCOs), and nonlinear dynamics.[17–20] These interesting physical phenomena are associated with the formation of energy "minibands", which enable electrons to perform Bloch oscillations when a sufficiently high static field is applied along the SL axis. Also, the Bloch oscillations have received much attention for the potential to yield THz generation. However, no such devices have been realized to date because the formation of the electric-field domains (EFDs) in SLs.[21] It leads to space-charge instability which inhibits the Bloch oscillations, and the value of frequency is difficult to reach THz. To solve this problem, many constructive proposals have been proposed.[22–26] One suggestion is to stack a few short SLs,[22] where EFDs are not able to form. These short SLs are separated by heavily doped material, and an increase in terahertz transmission at dc bias has been observed. Another scheme is the dc–ac-driven SLs, with the SLs biased in a negative differential velocity (NDV) region.[16,20] The initial THz ac pump is used to stabilize the distribution of EFDs and it can be gradually turned off when THz oscillation has been established in SLs. Yet another nonlinear circuit model is used to simulate the electric field domain suppression.[23] However, the model does not consider the electron tunneling transport that plays an important role in SLs behavior, and therefore the current self-oscillations are not observed. While the suppression of field domains has been reported, it is still not clear by now that whether these effects may be useful to establish THz devices on the basis of semiconductor SLs. On the other hand, the travelling field domains in weakly coupled SLs cause self-generated current oscillations under dc electric fields. The oscillation frequency can change from hundreds of kHz to several GHz over wide temperature ranges including room temperature. Then, some researchers start to consider how to use the field domains to generate THz wave.[24] These behaviors crucially depend on the SL configuration (widths of wells and barriers, number of SL periods, and boundary conditions in the contact regions), the doping density and the driven external fields.[25] Recently, the electrons behaviors in SLs have just been reported both experimentally and theoretically when a transverse magnetic field is applied.[26–28] However, up to now

*Project supported by the National Natural Science Foundation of China (Grant Nos. 11047108, 11005003, U1204115, and 11005002), the Fund from the Science and Technology Department of Hennan Provice, China (Grant No. 112300410183), and the Science Foundation from the Education Department of Henan Province, China (Grant No. 2011B140002).

†Corresponding author. E-mail: kuiziyang@126.com

© 2013 Chinese Physical Society and IOP Publishing Ltd

there has been no a detailed theoretical analysis, and therefore a comprehensive study is needed.

In this paper, we pay attention to the influence of magnetic fields on electron dynamics in weakly coupled GaAs/AlGaAs SLs. The static current–voltage characteristic curve as a function of magnetic fields B is plotted. In the curve, there exists NDV which is always related to the instability of system similar to the Gunn effect in n-GaAs. Controlled by the magnetic fields, the NDV region is changed, which implies that electrons in SLs will exhibit different oscillational behaviors. Indeed, three distinct results are observed with increasing magnetic fields. As shown in Fig. 2(a), the state of system with a lower doping density transfers from stationary state to oscillationary state. Corresponding to Fig. 2(b), we choose an intermediate value of doping density, the state changes from oscillationary to stationary. For a larger value of doping density shown in Fig. 2(c), the state varied between oscillationary and stationary. To give a detailed explanation, the phase diagrams of the SSCOs regime are plotted in the applied voltage and the doping density ($U_{\rm dc}-\lambda$) plane for various B values. Furthermore, the distribution of the electric-field domain along the SLs is plotted. We find the structure of the domain is almost uniform for a lower doping density, and no domain occurs in superlattices.

The rest of this paper is organized as follows. In Section 2, we briefly provide the model which has depicted the SL dynamics successfully. The simulated results which are obtained by solving the model numerically are summarized and discussed in Section 3. In Section 4 we present the dynamics driven by additional ac signals. Finally, we present our conclusion in Section 5.

2. Discrete rate equation model

The discrete rate equation model that we employ for the simulations below has been developed over the past several years and has proven to be useful to model experimental results with good accuracy.[7,29] The nonlinear charge transport in SLs can be described by the electron density $n_i(t)$ in the i-th well, and the average electric field $F_i(t)$ across the i-th period. According to the discrete Poisson equations, the voltage bias conditions and the Ampere's law, the governing equations for the SLs are given as follows:

$$(F_i - F_{i-1}) = \frac{e}{\varepsilon}(n_i - N_{\rm D}), \tag{1}$$

$$l\sum_{i=1}^{N} F_i = U(t), \tag{2}$$

$$\varepsilon\frac{{\rm d}F_i}{{\rm d}t} + J_{i\to i+1} = J(t), \tag{3}$$

where $i = 1,2,\ldots,N$ is the well index; ε, e, $N_{\rm D}$, and l are the well permittivity, the electron charge, the two-dimensional (2D) doping density in the wells, and the SL period, respectively. The total applied voltage $U(t)$ in Eq. (2) can be written as $U(t) = U_{\rm dc}\{1 + A\sin(2\pi f_{\rm d}t)\}$ with $U_{\rm dc}$ is the dc voltage, A and $f_{\rm d}$ are the relative amplitude and driving frequency of an ac microwave signal.

Equation (3) shows that the total current density $J(t)$ consists of a displacement current and the tunneling current $J_{i\to i+1}$=$en_i v_{\rm d}(F_i)$. The tunneling current is determined by electrons tunneling from the ground states E_1^{i-1} in $(i-1)$-th well to the ground states $(E_1^{i-1} - E_1^i)$, the first excited states $(E_1^{i-1} - E_2^i)$ and the second excited states $(E_1^{i-1} - E_3^i)$ of the i-th well. Applying a transverse magnetic field parallel to x axis, an electron travels the tunneling distance l from one well to the next, which picks up the transverse momentum $\hbar k_y = eBl$ due to the Lorentz force, $\hbar$ and k_y are the Planck constant and wave vector in the y-axis direction, respectively. This results in an energy transferring from the z direction to the y direction, $\Delta E = e^2B^2l^2/(2m^*)$, where m^* is the effective mass. To maintain the resonant condition this energy must be compensated by an additional electric field $\Delta F = \Delta E/(el)$. Thus, the resonant peak electric field shifts to a higher value $F = F_{1-2} + \Delta F$. The electrons drift velocity $v_{\rm d}(F_i)$ is a sum of Lorentzian functions centered at the resonant field values $F_{1-2} = (E_j^i - E_1^{i-1})/(el)$ which strongly depends on the electric field and the magnetic field, and it is expressed as

$$v_{\rm d}(F_i) = \sum_{j=1}^{n} \frac{\dfrac{\hbar^3 l(\gamma_1^i + \gamma_j^i + 2\alpha\hbar^2 k_{\rm f}k_y/m^*)}{2m^{*2}} T_j(E_1^i)}{(E_j^i - E_1^i + eF_i l - e^2l^2B^2/2m^*)^2 + (\gamma_1^i + \gamma_j^i + 2\alpha\hbar^2 k_{\rm f}k_y/m^*)^2}. \tag{4}$$

In this formula, $\gamma_j^i = 8$ meV indicates the scattering width, $\alpha = 0.16$ is the model parameter, $k_{\rm f} = \sqrt{2m^*E_{\rm F}/\hbar^2}$ with $E_{\rm F} = 5$ meV is the energy of Fermi surface, T_j is proportional to the dimensionless transmission probability across the i-th barrier.

The assumed phenomenological boundary condition gives

$$\frac{\varepsilon(F_i - F_0)}{el} = n_1 - N_{\rm D} = \delta N_{\rm D}, \tag{5}$$

where δ accounts for the excess electron density in the first well due to the tunneling from the highly doped contact region.

The current density $J(t)$ in the external circuit under voltage bias condition can be obtained from the time derivative of Eq. (2) and the Ampere's law may be written in the following form:

$$J(t) = c_{\rm U}\frac{{\rm d}U}{{\rm d}t} + \frac{e}{N}\sum_{j=1}^{N} n_j v_{\rm d}(F_i), \tag{6}$$

where $c_{\rm U} = \varepsilon/(lN)$ is the intrinsic SL capacitance per unit cross-sectional area.

To carry out numerical simulation of the discrete rate equation model, the following dimensionless variables are used: $\Phi_i = F_i/F_{1-2}$, $F_{1-2} = (E_2^i - E_1^{i-1})/(el)$, $n_0 = \varepsilon F_{1-2}/(el)$, $\lambda = N_{\rm D}/n_0$, $t_{\rm tun} = l/v_{\rm d}(F_{1-2})$, $\tau = t/t_{\rm tun}$, $w = 2\pi f_{\rm d} t_{\rm tun}$, $V = U_{\rm dc}/(F_{1-2}lN)$, and $a = AV$.

Now substituting Eqs. (1) and (6) into Eq. (2), N dimensionless equations are obtained as

$$\frac{{\rm d}\Phi_i}{{\rm d}\tau} = \frac{1}{N}\sum_{j=1}^{N} v_{\rm d}(\Phi_j)[\Phi_j - \Phi_{j-1} + \lambda] - v_{\rm d}(\Phi_i)[\Phi_i - \Phi_{i-1} + \lambda] + aw\cos(w\tau). \tag{7}$$

Together with Eq. (4) and the initial condition $\Phi_i(0) = V$, we solve Eq. (7) by the fourth order Runge–Kutta method.

3. Dependence of dynamics on magnetic field

In this section, we discuss the effects of the SLs under a transverse magnetic field. A weakly coupled GaAs/AlAs (n-doped/undoped) SL is considered to be composed of 40 periods. The widths of each GaAs quantum well and AlAs barrier are 9.0 nm and 4.0 nm, respectively, which implies that the subband energies are $E_1 = 44$ meV, $E_2 = 180$ meV, and $E_3 = 410$ meV. The 2D doping density in each quantum well is $N_{\rm D}$=1.15×10^{11} cm^{-2} and the temperature is maintained at $T = 5$ K. In Fig. 1, we plot the normalized electron drift velocity as a function of the applied dc voltage and the magnetic field. The solid, dash, and dot lines indicate the curves for $B = 0$, 6, and 12 T, respectively. Clearly, three NDV regions are observed, which means the instability of the system which is expected to display interesting nonlinear behaviors.

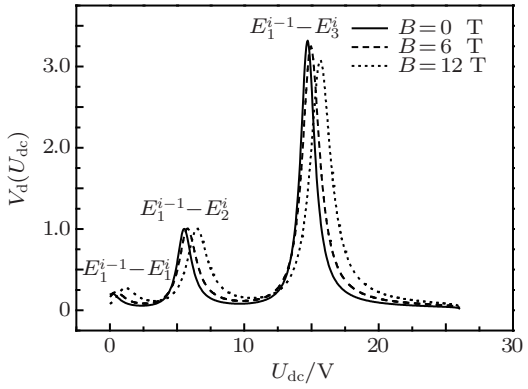


Fig. 1. Calculated normalized electron drift velocities versus applied dc voltage at three different magnetic fields: $B = 0$, 6, and 12 T.

The peak velocity location corresponding to the occurrence of resonant tunneling of electrons shifts to a higher voltage, i.e., $U_{\rm dc} = (F_{1-2} + \Delta F) \times N \times l$, with magnetic field increasing.

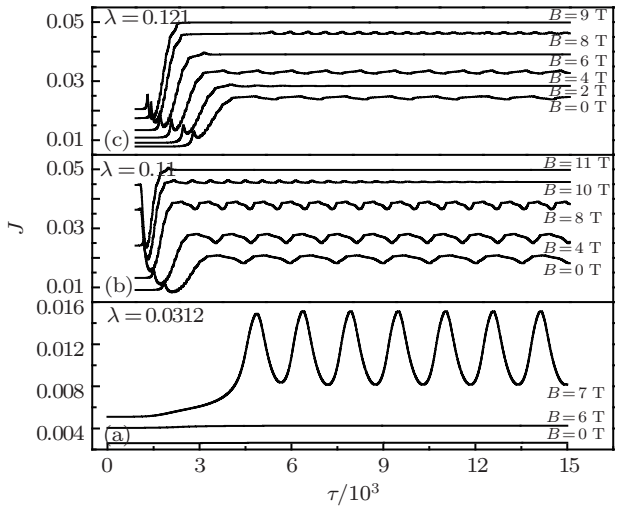


Fig. 2. Temporal evolutions of the current density controlled by magnetic fields for different doping densities: (a) λ=0.0312 (b) λ=0.11, and (c) λ=0.121. Here the current density is in units of $en_0v_{\rm d}(F_{1-2})$ and time τ is in units of $t_{\rm tun}$.

The numerical results are supplied by solving Eq. (6) to study the system dynamical behaviors. In our calculation, the first NDV region is concerned and the pure dc voltage ($a = 0$) is biased in the NDV region. Three different cases are considered, which is enough to depict the physical phenomenon. The initial condition is chosen to be (a) $U_{\rm dc} = 1.545$, (b) $U_{\rm dc} = 1.099$, and (c) $U_{\rm dc} = 1.632$, respectively. Figures 2(a)–2(c) show the temporal evolutions of the current density J for different doping densities. The current density starts from τ=0, after a short time, it runs to dynamical state or oscillational state controlled by the external magnetic field. The current density is in units of $en_0v_{\rm d}(F_{1-2})$ and time τ is in units of $t_{\rm tun}$. In the case of a lower doping density λ=0.0312 as shown in Fig. 2(a), no current oscillations are observed when the magnetic field B varies from 0 T to 6 T. As $B = 7$ T, the SSCOs occur, which indicates the periodic motion of the charge dipole layers across all or part of the SLs formed with the increasing B. For the larger value such as λ=0.11 corresponding to Fig. 2(b), a contrary result is obtained. Affected by the magnetic field, the state of the system transfers from dynamical to stationary. Below $B = 8$ T, the current exhibits SSCOs, which indicates that the system is in dynamical state. Above $B = 10$ T, after some transient periods of the order of $t_{\rm tun}N$, the system runs to a stationary state which corresponds to a field configuration with a high-field domain near the collector and a low-field domain near the emitter. The two domains are separated by a charge accumulation layer that is mostly confined to two adjacent quantum wells. As the doping density increases to λ=0.121 as shown in Fig. 2(c), the calculated result is more

complicated. When the magnetic field $B = 0$, 4, and 8 T, each current shows undamped temporal evolution of current. While the cases for $B = 2$, 6, and 9 T each exhibit no oscillation after a short transient at the beginning, which means the formation of the static domain in SLs. So the system state switches between dynamic and stationary with the change of the magnetic field. Further increasing the magnetic field B (> 9 T), no SSCOs are observed and only the static EFDs are formed in SLs.

Figures 2(a)–2(c) show that the system state is greatly dependent on the doping density and magnetic field. Choosing different doping densities, the system exhibits various behaviors dominated by the magnetic field. The detailed explanation is given as follows. In Figs. 3(a)–3(d), the phase diagrams of the SSCO regime are plotted in the applied voltage and the doping density ($U_{\rm dc} - \lambda$) plane for various B values. The doping density λ and the bias $U_{\rm dc}$ are in units of n_0 and volt, where the shadowed areas correspond to SSCO regimes, which shows the system has an unstable solution. The number of the branches in phase diagram is only 21, which is not equal to the number of the SL wells. The reason is attributed to the special choice of the model parameters. One then notices that the SSCO regime has been steadily squeezed by increasing magnetic field B. For $B = 0$ T, the boundaries of the shadowed areas for the doping density and the dc bias are in the ranges $(0.03255, 0.1362)$ and $(0.1728, 2.1276)$, respectively. At the external magnetic field $B = 3$ T, the SSCO solution exists just in the regions of $\lambda \in (0.03195, 0.1345)$ and $U_{\rm dc} \in (0.23085, 2.187)$. Increasing the magnetic field to $B = 6$ T, the boundary of the doping density becomes between 0.0317 and 0.1303 while the bias changes from 0.324 to 2.2896. As $B = 9$ T, the SSCO requires that $\lambda \in (0.03035, 0.1189)$ and $U_{\rm dc} \in (0.6725, 2.649)$. In the case of B equal to 10 T, the SSCOs can be observed in the regions of $\lambda \in (0.03011, 0.1095)$ and $U_{\rm dc} \in (0.7784, 2.776)$, which is not shown in Fig. 3. Comparing the numerical results, the minimum $\lambda_{\rm min}$ and the maximum $\lambda_{\rm max}$ of the doping density in the shadowed areas become smaller and smaller, while the value of the applied voltage becomes more and more big. With the doping density λ=0.0312, the λ value is outside the shadowed areas until the magnetic field $B = 7$ T. Thus, the system state changes from stationary to dynamically dependent on magnetic field. For λ=0.11, an opposite result is obtained, and the system state varies from dynamical to stationary, controlled by the magnetic field. For the case of λ=0.121, the λ value is just in the branch areas which shifts to a higher field affected by the magnetic field. Therefore, the system state transfers between the stationary state and dynamical state when the dc bias is fixed at $U_{\rm dc} = 1.632$. As $B > 9$ T, λ=0.121 is out of the range $\lambda \in (0.03035, 0.1189)$, and the SSCOs disappear. The diagrams of λ and $U_{\rm dc}$ each as a function of the magnetic field B is plotted in Figs. 4(a)–4(b), where $\lambda_{\rm min}$, $\lambda_{\rm max}$, $U_{\rm min}$, and $U_{\rm max}$ denote the maximum and minimum of the doping density and dc voltage values in the SSCO regime for each magnetic field B, respectively. From Fig. 4(a), we find that $\lambda_{\rm max}$ and $\lambda_{\rm min}$ drop with B increasing, but $\lambda_{\rm max}$ decreases more sharply. Therefore, the difference between $\lambda_{\rm max}$ and $\lambda_{\rm min}$ becomes smaller. As for $U_{\rm max}$ and $U_{\rm min}$, the two values increase simultaneously with B increasing, and the difference

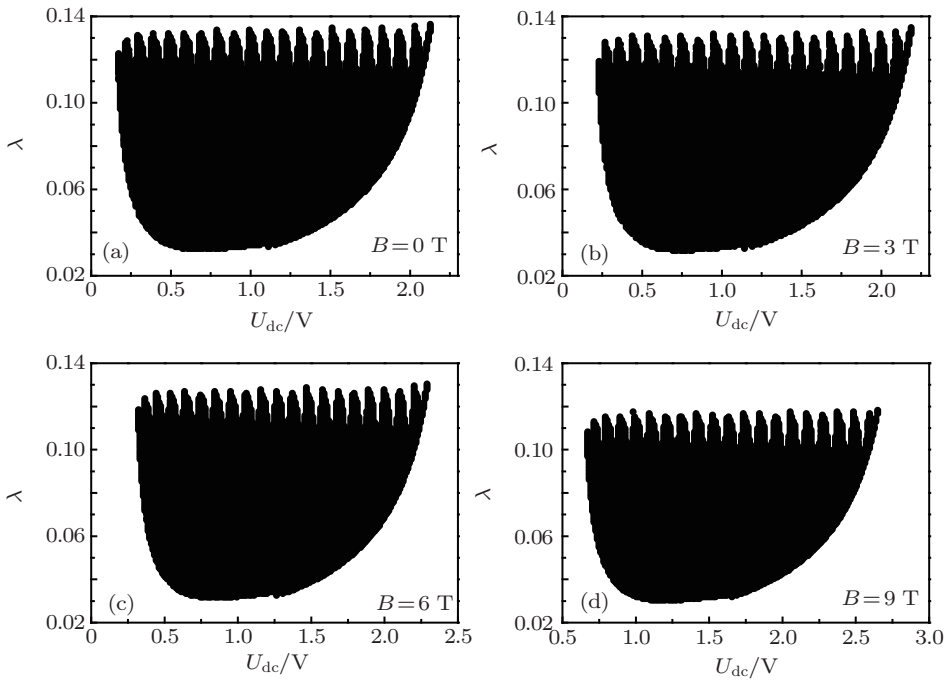


Fig. 3. Phase diagrams in the applied voltage and the doping density ($U_{\rm dc} - \lambda$) plane for (a) $B = 0$ T, (b) $B = 3$ T, (c) $B = 6$ T, and (d) $B = 9$ T. Here λ is in units of n_0 and $U_{\rm dc}$ is in units of volt. The system inside the shadowed area will have an SSCO solution.

$(U_{\max} - U_{\min})$ is almost unchanged. Thus, the SSCO regime becomes smaller with the increase of B, which is mainly due to the change of the doping density range. The simulation result can be explained as follows. The SSCO is always related to the formation of an unstable EFD which requires a sufficient high doping density in SLs. Due to the tunneling electrons under the magnetic field, the motion of carriers is changed by the Lorentz force, which leads to the accumulation of the carriers. That is to say, the magnetic field B is in favor of the formation of the EFDs. For a lower doping density near $\lambda_{\min}$, the unstable EFDs are formed under the applied magnetic field, and the system state transfers from stationary state to oscillationary state. As for a higher doping density close to the $\lambda_{\max}$ in the SSCO regime, the magnetic field contributes to the formation of the EFDs, and the SSCOs disappear with B increasing.

To make the process clearer, the spatiotemporal evolutions of EFDs are plotted in Figs. 5 and 6 which correspond to three cases. The colorbar indicates the value of the electric field. At the beginning, $\tau = 0$, the distribution of the electric field is uniform which is set as the initial condition. Then, the applied dc voltage is turned on, after a short time, the system reaches a new state. Figure 5(a) shows the case of $B = 0$ and λ=0.0312. Strangely, the distribution of the electric field is almost uniform which can be judged by the colorbar, the colors are almost the same. As the magnetic field is added to $B = 7$ T shown in Fig. 5(b), an EFD is generated and moves toward the other contact of the SLs. Depending on the external dc bias, it may or may not reach the end of the SL before it disappears and a new domain is formed. The periodic propagation of the domain leads to current oscillations as shown in Fig. 2(a). As λ=0.0312, it is lower than the critical value 0.03255 as shown in Fig. 2(a), so no EFD occurs. Increasing the magnetic field, the motion of carriers is changed by the Lorentz force, which leads to the accumulation of the carriers, and the formation of the EFD is possible at $B = 7$ T. Figure 6 shows the distributions of unstable and stable EFDs, which correspond to SSCO solution and stable state of the system. The stable EFD is split up into two regions with high and low electric-field domain along the SLs.

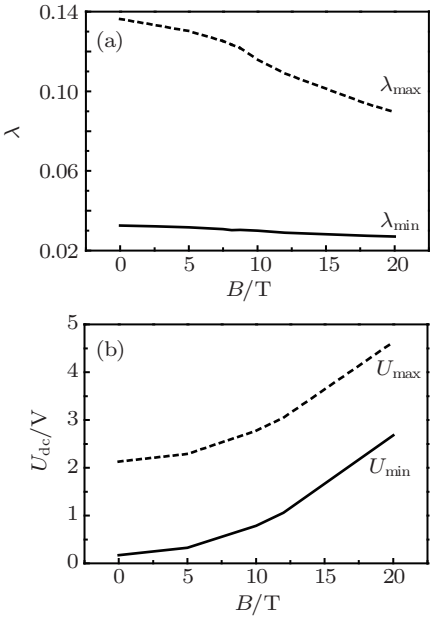


Fig. 4. Variations of the doping density λ range (a) and the applied voltage U_{dc} range (b) with magnetic field B.

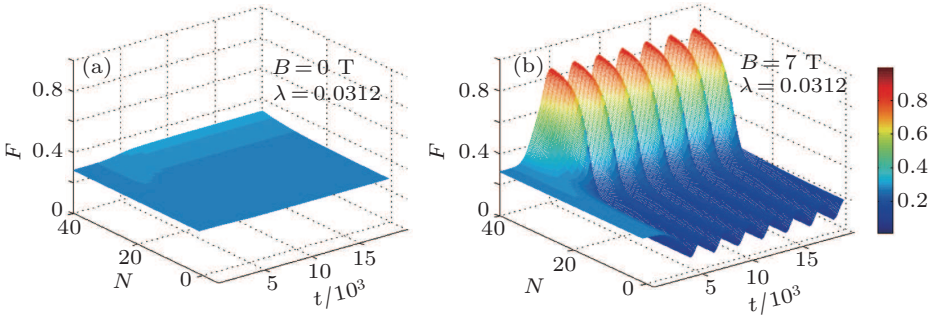


Fig. 5. (color online) Spatiotemporal evolutions of the electric field at (a) $B = 0$ T, λ=0.0312 and (b) $B = 7$ T, λ=0.0312. Quantum well index is denoted by N. The electric field is in units of F_{1-2} and time τ is in units of t_{tun}.

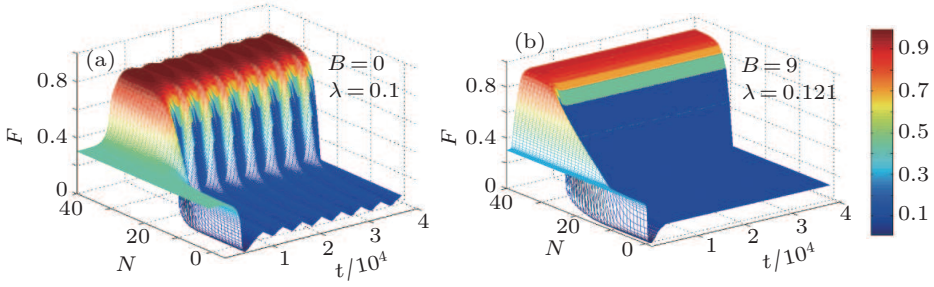


Fig. 6. (color online) Spatiotemporal evolutions of the electric field which corresponds to SSCO state and stable state in SLs. (a) $B = 0$ T, λ=0.1; (b) $B = 9$ T, λ=0.121.

4. Complex dynamics driven by ac voltage

The dynamics of the system driven by the ac voltage is investigated. The ac signal can be written as $U(t) = U_{\rm dc}\{1 + A\sin(2\pi f_{\rm d}t)\}$. Due to the coupling between the inherent SSCO and the external ac signal, the system exhibits interesting nonlinear dynamics when the amplitude A and the driving frequency $f_{\rm d}$ are changed. In our calculations, we take $B = 6$ T for example to describe the system behaviors. The parameters are set to be $\lambda = 0.08$, $U_{\rm dc} = 1.7$ V, and $A = 0.15$.

In order to detect the system behaviors, the Poincaré map and the corresponding phase diagrams each as a function of driving frequency $f_{\rm d}$ are plotted in Fig. 7 and Fig. 8. We sample the current density J_n at $T_n = nT_{\rm d}$, $n = 1, 2, \ldots$ with $T_{\rm d} = 1/f_{\rm d}$. For each $f_{\rm d}$, we calculate $J_n = J(nT_{\rm d})$ until the solution becomes stable within a 10^{-5} accuracy. At that time, we stop the simulation and record all the values of J_n. From Fig. 6 one can see that the system displays period-1 oscillation which corresponds to one point in Poincaré map at the beginning of $0.5 < f_{\rm d}/f_0 < 0.87$, where $f_0 = 1/(180.5t_{\rm tun})$. In the range of $0.87 \leq f_{\rm d}/f_0 < 1.44$, period-2 oscillation can be found by judging two points in Poincaré map. Further increasing the driving frequency to $1.44 \leq f_{\rm d}/f_0 < 2.5$, different nonlinear dynamics such as period-n and chaos occurs. The phase portraits in the $(U_{\rm dc}, J)$ plane are plotted in Figs. 8(a)–8(f) with driving frequencies: $f_{\rm d}/f_0 = 0.75$ (a), 0.93 (b), 1.25 (c), 1.84 (d), 1.91 (e), and 2.1 (f), respectively.

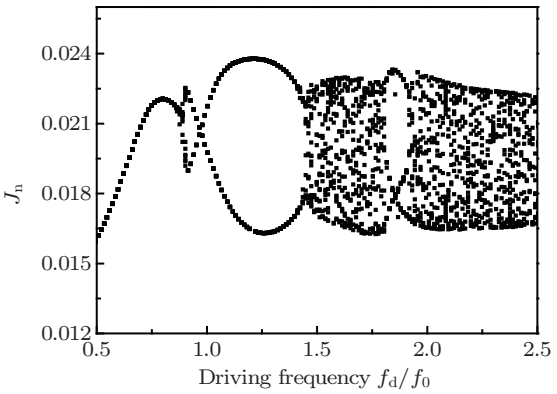


Fig. 7. Poincaré bifurcation diagram of the current density J_n as a function of the driving frequency $0.5 < f_{\rm d}/f_0 < 2.5$ with the doping density $\lambda = 0.08$.

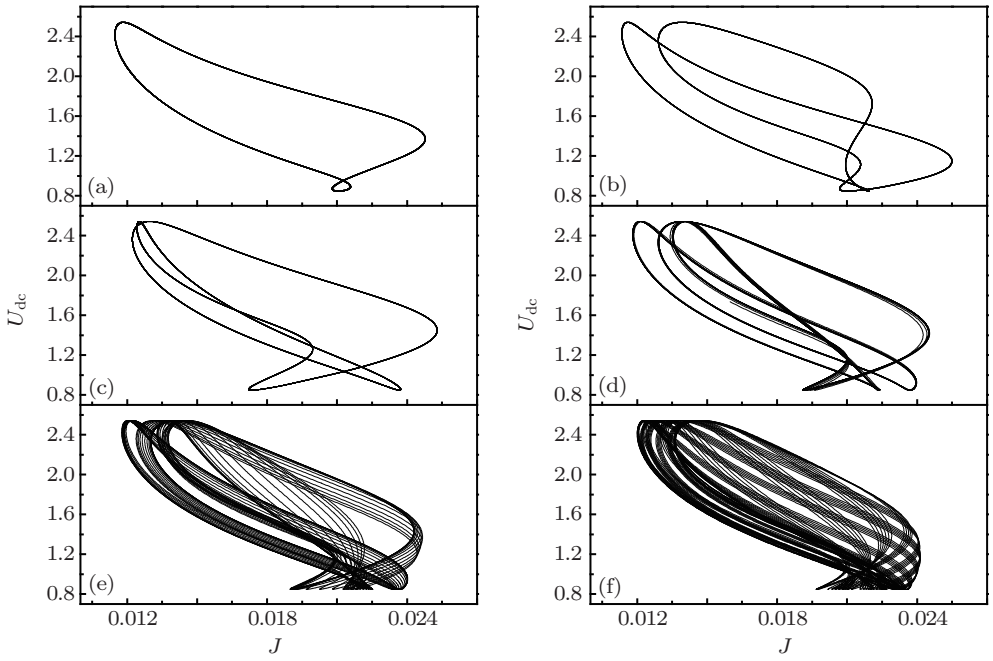


Fig. 8. Phase portraits in the $(U_{\rm dc}, J)$ plane with different ratios of $f_{\rm d}/f_0$: (a) 0.75, (b) 0.93, (c) 1.25, (d) 1.84, (e) 1.91, and (f) 2.1.

5. Conclusion

How the magnetic field affects the electrons transport in weakly coupled GaAs/AlAs semiconductor superlattices is studied. The main transport physical mechanism is sequential tunneling. We find that the system state strongly relies on two parameters, one is the doping density, and the other is the magnetic field. For a small doping density, i.e., λ=0.0312, it is not sufficient to form an EFD in SLs and no SSCO occurs. Adding the magnetic field B to 7 T, the stronger Lorentz force induces the formation of EFD, of which the periodic motion results in the SSCOs. Fixing the doping densities λ=0.11 and λ=0.121, the electronic behaviors are changed with the increases of magnetic field and the system state transfers between the stationary state and oscillationary state. The structure of the EFD in superlattices is plotted for different doping densities, which

shows that the dynamics is attributed to the control parameter. Driven by the ac voltage, the system exhibits interesting nonlinear dynamics including period-1, period-2, and chaos due to the competition between the internal signal and driven signal. The Poincaré map and the corresponding phase diagrams are given in the text.

References

[1] Esaki L and Tsu R 1970 *IBM Journal of Research and Development* **14** 1
[2] Wacker A 2002 *Phys. Rep.* **357** 1
[3] Xu H D and Teitsworth S W 2007 *Phys. Rev. B* **76** 235302
[4] Wang W, Qi X and Yue Y 2011 *Chin. Phys. B* **20** 017502
[5] Gong C C, Fan G H, Zhang Y Y, Xu Y Q, Liu X P, Zheng S W, Yao G R and Zhou D T 2012 *Chin. Phys. B* **21** 068505
[6] Yang L, Hu G Z, Hao Y, Ma X H, Quan S, Yang L Y and Jiang S G 2010 *Chin. Phys. B* **19** 047301
[7] Bonilla L L, Escobedo R and Dell'Acqua G 2006 *Phys. Rev. B* **73** 115341
[8] Amann A and Schöll E 2005 *Phys. Rev. B* **72** 165319
[9] Yu X X, Xie Y E, Ouyang T and Chen Y P 2012 *Chin. Phys. B* **21** 107202
[10] Bonilla L L and Grahn H T 2005 *Rep. Prog. Phys.* **68** 577
[11] Rasulova G K, Brunkov P N, Egorov A Y and Zhukov A E 2009 *J. Appl. Phys.* **105** 033711
[12] Hizanidis J, Balanov A, Amann A and Schöll E 2006 *Phys. Rev. Lett.* **96** 244104
[13] Wu B Y, Duan S Q and Zhao X G 2004 *Chin. Phys.* **13** 1544
[14] Feng W 2012 *Chin. Phys. B* **21** 037306
[15] Zwolak M, Ferguson D and DiVentra M 2003 *Phys. Rev. B* **67** 081303
[16] Hyart T, Alekseev Kirill N and Thuneberg Erkki V 2008 *Phys. Rev. B* **77** 165330
[17] Wang J, Hu Bambi, Zheng Z G and Li Z G 2011 *Phys. Rev. B* **83** 155306
[18] Dreisow F, Szameit A, Heinrich M, Pertsch T, Nolte S, Tünnermann A and Longhi S 2009 *Phys. Rev. Lett.* **102** 076802
[19] Arana J I, Bonilla L L and Grahn H T 2010 *Phys. Rev. B* **81** 035322
[20] Cao J C 2002 *Chin. Phys. Lett.* **19** 1519
[21] Xu H D, Amann A, Schöll E and Teitsworth Stephen W 2009 *Phys. Rev. B* **79** 245318
[22] Savvidis P G, Kolasa B, Lee G and Allen S J 2004 *Phys. Rev. Lett.* **92** 196802
[23] Daniel E, Gilbert B, Scott J and Allen S 2003 *IEEE Trans. Electron Dev.* **50** 2434
[24] Greenaway M T, Balanov A G, Schöll E and Fromhold T M 2009 *Phys. Rev. B* **80** 205318
[25] Bulashenko O M, Garcia M J and Bonilla L L 1996 *Phys. Rev. B* **53** 10008
[26] Sun B Q, Wang J N and Jiang D S 2005 *Semicond. Sci. Technol.* **20** 947
[27] Wang C and Cao J C 2005 *Chaos* **15** 013111
[28] Yury A M, Vladimir N M and Maxim P T 2006 *Physica E* **32** 297
[29] Wang X R, Wang J N, Sun B Q and Jiang D S 2000 *Phys. Rev. B* **61** 7261